JOC Article
pubs.acs.org/joc

Cascade [1,3]-Sigmatropic Rearrangements of Ketene *O*,*O*-Acetals: Kinetic and DFT Level Mechanistic Studies

Perla Y. López-Camacho,[†,‡] Pedro Joseph-Nathan,[†] Bárbara Gordillo-Román,[†] Oscar R. Suárez-Castillo,[§] and Martha S. Morales-Ríos*[,†]

[†]*Departamento de Química, and* [‡]*Departamento de Farmacología, Centro de Investigación y de Estudios Avanzados del Instituto Politécnico Nacional, Apartado 14-740, México, D. F., 07000 Mexico, and* [§]*Centro de Investigaciones Químicas, Universidad Autónoma del Estado de Hidalgo, Apartado 1-622, Pachuca, Hidalgo, 42001 Mexico*

smorales@cinvestav.mx

Received December 7, 2009

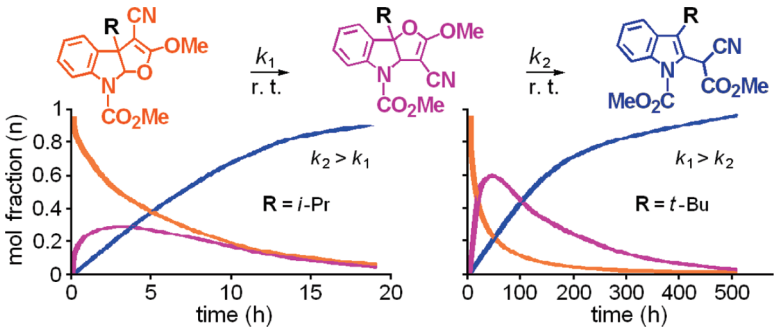

The regioisomeric α-cyano ketene-*O*,*O*-dialkyl acetals **2a**−**e** and **4a**−**e**, sequential intermediates in the diazomethane induced conversion of indole α-cyano-γ-lactones **1a**−**e** to 2-indolyl cyanomalonates **5a**−**e**, were isolated and characterized. Formation of the steady-state intermediate cycloprop-[*b*]indoles **3a**−**e** was evidenced by means of NMR and confirmed by the X-ray structure of **3c**, demonstrating that the formation of **5a**−**e** from **2a**−**e** proceeds through two consecutive and one parallel unimolecular steps, with intermediates **3a**−**e** formed in reversible processes. Evidence that the reversible reactions proceed via [1,3]-rearrangements is presented. The steady-state kinetic approach applied to intermediate **3** allowed a minimal two consecutive step **2** → **4** → **5** kinetic model, in which the steric bulkiness of the alkyl substituent affects strongly the associated rate constants, k_1 and k_2, inverting the rate-determining step. The solvation effects enhanced the feasibility of these skeletal rearrangements as they stabilized the transition states to a great extent. The experimental determined thermodynamic parameters and DFT calculations suggest that these cascade rearrangements occur through [1,3]-sigmatropic mechanisms, in which asynchronous bond reorganization processes via four membered pseudopericyclic transition states are highly favorable.

Introduction

Involvement of an unexpected skeletal reorganization has attracted the attention of organic chemists not only for the search for synthetic applications but also to perform mechanistic studies. In this respect, experimental and theoretical studies concerning ketene acetal rearrangements are an active area of chemical research, since they have found considerable applications in the natural and unnatural product synthesis.[1] Among ketene acetals, those derived from esters are the most common and best investigated reactive precursors in the Claisen and Ireland−Claisen sigmatropic rearrangements.[2,3]

*To whom correspondence should be addressed. Tel: +(52 55)5747 7112. Fax: +(52 55)5747 7137.

(1) For a review of applications of ketene acetal rearrangement in synthesis, see: Tadano, K. In *Studies in Natural Products Chemistry*; Rahman, A.-U., Ed.; Elsevier: Amsterdam, 1992; pp 405−455.

(2) For reviews of asymmetric Claisen rearrangement, see: (a) Enders, D.; Knopp, M.; Schiffers, R. *Tetrahedron: Asymmetry* **1996**, *7*, 1847–1882. (b) Ito, H.; Taguchi, T. *Chem. Soc. Rev.* **1999**, *28*, 43–50.

(3) For a review on Ireland and related Claisen rearrangement, see: Chai, Y.; Hong, S.-p.; Lindsay, H. A.; McFarland, C.; McIntosh, M. C. *Tetrahedron* **2002**, *58*, 2905–2928.

Published on Web 02/24/2010 DOI: 10.1021/jo902520z

However, contrary to the widely recognized [3,3]-sigmatropic rearrangement of ketene acetals, the [1,3] process is a rare event witnessed previously in a few cases of acyclic and semicyclic enolates derived from benzyl esters, in which the intervention of the typical [3,3] process is energetically unfavorable.[4] In these cases, the 3,3-shift can be markedly affected by substantial loss of the aromatic π-electron delocalization of the benzyl group upon migration, which is a requirement for this type of reaction to occur. In contrast, the benzyl group presumably could stabilize either radical intermediates or charge build-up in the transition state for the concerted 1,3-shift. In addition, there exist only two isolated reports in the literature involving [1,3]-sigmatropic rearrangements of silyl lactone enolates to provide contracted carbocyclic ring systems with high diastereoselectivity.[5] As a consequence, little or no information exists to date about those electronic and steric factors on rates of [1,3]-sigmatropic rearrangements of ketene acetals and the nature of the transition states for such processes.

Studies in the field of furoindolines chemistry has been of great interest in our laboratory in the past few years.[6] Herein, we report the first systematic study of the steric effects on the cascade [1,3]-sigmatropic rearrangement of β-alkyl-substituted ketene-*O*,*O*-acetals and evidence on the nature of the transition states for such processes is discussed.

Results and Discussion

Synthesis. The studied α-cyano-γ-lactones **1a**−**e** (Figure 1), varying over a significant range in terms of the size of the alkyl group (R = Me, Et, Bn, *i*-Pr, *t*-Bu) on the C3a bridgehead carbon, were conveniently synthesized from a 2-hydroxyindolenine via chelation-controlled 1,4-conjugated addition of Grignard reagents[7] and subsequent lactonization in yields ranging from 74% for R = *i*-Pr to 21% for R = *t*-Bu.[7b] The low yield of **1e** is due to a greater steric hindrance at the newly formed quaternary carbon center.[8] Starting substrate **1c**, appearing in $CDCl_3$ solution as an equilibrated racemic mixture of *cis*-fused 11:2 endo/exo diastereoisomers,[9] was prepared in one pot from *Z*-1-carbomethoxy-2-hydroxy-3-indolinylidenecyanoacetate[10] with benzylmagnesium bromide.

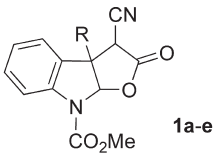

R: **a** = Me, **b** = Et, **c** = Bn, **d** = *i*-Pr, **e** = *t*-Bu

FIGURE 1. Structural formulas for α-cyano-γ-lactones **1a**−**e**.

Cascade Reactions with Diazomethane. The α-cyano-γ-lactones of type **1** revealed in solution and at room temperature a dynamic stereochemistry governed by the steric preferences of the cyano group at the C3 stereocenter.[11] Since the interconversion of the endo/exo isomers of **1** is expected to involves passage through an enol tautomer, reaction of **1a**−**e** with diazomethane could give the desired ketene *O*,*O*-acetals.[12] Compounds **1a**−**e** were treated with an excess of freshly prepared diazomethane[13] in ether for 5 min at room temperature. The GC−mass spectral analysis of the reaction crude exhibited in all cases a clean molecular ion peak $[M]^+$ shifted by 14 Da with respect to that of starting material, which could be ascribed, at first glance, to the expected ketene *O*,*O*-acetals **2a**−**e**. NMR analysis of the crude reaction mixture conducted in acetone-d_6 however, evidenced the inherent instability of the ketene *O*,*O*-acetals **2**.[14] Thus, whereas the ^{1}H NMR spectra of **2d** and **2e** gave a single set of signals, which agreed very well with the proposed structures, those owing to **2a**−**c** allowed us to detect one or two additional isomeric species which, although not identified, had ^{1}H NMR spectra resembling those of **2**. To our surprise, standing neat **2a** under ambient conditions for one week spontaneous and quantitatively rearranged to the thermodynamically more stable 2-indolylcyanomalonate **5a**, reveling one of the two previously detected isomeric species.

In addition, when **2c** was standing neat for several weeks, it furnished a mixture of starting ketene *O*,*O*-acetal **2c**, the expected 2-indolylcyanomalonate **5c**, and a compound whose ^{13}C NMR analysis showed the presence of signals most likely attributable to a regioisomer of **2c**, the corresponding inverted ring-fusion furo[3,2-*b*]indole **4c**, than to the ring-contracted cyclopropyl scaffold structure **3c**.[15]

(4) (a) Arnold, R. T.; Kulenovic, S. T. *J. Org. Chem.* **1980**, *45*, 891–894. (b) Shiina, I.; Nagasue, H. *Tetrahedron Lett.* **2002**, *43*, 5837–5840. (c) Burger, K.; Gaa, K.; Geith, K.; Schierlinger, C. *Synthesis* **1989**, 850–855. (d) Shishido, K.; Shitara, E.; Fukumoto, K. *J. Am. Chem. Soc.* **1985**, *107*, 5810–5812. (e) Susuki, T; Inui, M.; Hosokawa, S.; Kobayashi, S. *Tetrahedron Lett.* **2003**, *44*, 3713–3716. For a review which includes the [1,3]-sigmatropic rearrangement of ketene acetals, see: Nasveschuk, C. G.; Rovis, T. *Org. Biomol. Chem.* **2008**, *6*, 242–244.

(5) (a) Danishefsky, S.; Funk, R. L.; Kerwin, J. F. *J. Am. Chem. Soc.* **1980**, *102*, 6891–6893. (b) Kahn, K. M.; Knight, D. W. *J. Chem. Soc., Chem. Commun.* **1991**, 1699–1701.

(6) (a) Morales-Ríos, M. S.; Suárez-Castillo, O. R.; García-Martínez, C.; Joseph-Nathan, P. *Synthesis* **1998**, 1755–1759. (b) Morales-Ríos, M. S.; Suárez-Castillo, O. R.; Alvarez-Cisneros, C.; Joseph-Nathan, P. *Can. J. Chem.* **1999**, *77*, 130–137. (c) Morales-Ríos, M. S.; Suárez-Castillo, O. R.; Joseph-Nathan, P. *J. Org. Chem.* **1999**, *64*, 1086–1087. (d) Morales-Ríos, M. S.; Suárez-Castillo, O. R.; Trujillo-Serrato, J. J.; Joseph-Nathan, P. *J. Org. Chem.* **2001**, *66*, 1186–1192. (e) Morales-Ríos, M. S.; Santos-Sánchez, N. F.; Joseph-Nathan, P. *J. Nat. Prod.* **2002**, *65*, 136–141. (f) Morales-Ríos, M. S.; Suárez-Castillo, O. R.; Joseph-Nathan, P. *Tetrahedron* **2002**, *58*, 1479–1484. (g) Morales-Ríos, M. S.; Santos-Sánchez, N. F.; Fragoso-Vázquez, M. J.; Alagille, D.; Villagómez-Ibarra, J. R.; Joseph-Nathan, P. *Tetrahedron* **2003**, *59*, 2843–2853. (h) Morales-Ríos, M. S.; Rivera-Becerril, E.; Joseph-NathanP. *Tetrahedron: Asymmetry* **2005**, *16*, 2493–2499. (i) Rivera-Becerril, E.; Joseph-Nathan, P.; Pérez-Alvarez, V. M.; Morales-Ríos, M. S. *J. Med. Chem.* **2008**, *51*, 5271–5284.

(7) (a) Morales-Ríos, M. S.; Bucio, M. A.; Joseph-Nathan, P. *Tetrahedron* **1996**, *52*, 5339–5348. (b) Morales-Ríos, M. S.; García-Martínez, C.; Bucio, M. A.; Joseph-Nathan, P. *Monatsh. Chem.* **1996**, *127*, 691–699. (c) Morales-Ríos, M. S.; Bucio, M. A.; García-Martínez, C.; Joseph-Nathan, P. *Tetrahedron Lett.* **1994**, *35*, 6087–6088. (d) Morales-Ríos, M. S.; Bucio, M. A.; Joseph-Nathan, P. *Tetrahedron Lett.* **1994**, *35*, 881–882.

(8) Rueping, M; Nachtsheim, B. J.; Moreth, S. A.; Bolte, M. *Angew. Chem., Int. Ed.* **2008**, *47*, 593–596.

(9) Based on the integration of the CH_2 AB proton signals: ^{1}H NMR (300 MHz, $CDCl_3$) δ 3.10 (endo), 3.35 (exo) ppm.

(10) Morales-Ríos, M. S.; Bucio-Vásquez, M. A.; Joseph-Nathan, P. *J. Heterocycl. Chem.* **1993**, *30*, 953–956.

(11) In these types of compounds, the equilibrium isomer distribution is solvent dependent; see: Morales-Ríos, M. S.; Suárez-Castillo, O. R.; Joseph-Nathan, P. *J. Chem. Soc., Perkin Trans. 2* **2000**, 769–775.

(12) Morales-Ríos, M. S.; López-Camacho, P. Y.; Suárez-Castillo, O. R.; Joseph-Nathan, P. *Tetrahedron Lett.* **2007**, *48*, 2245–2249.

(13) Arndt, F. *Organic Syntheses*; Wiley: New York, 1943; Vol. 2, pp 165−167.

(14) The solvent choice for NMR measurements was acetone-d_6 rather than $CDCl_3$ because the acidic character of the later resulted in reconverted cyano lactones **1a**−**e** in minor amounts, together with decomposition products.

(15) (a) For a ^{13}C NMR example of a furo[3,2-*b*]indole, see: Tsai, A.-I.; Lin, C.-H.; Chuang, C.-P. *Heterocycles* **2005**, *65*, 2381–2394. (b) For ^{13}C NMR examples of cycloprop[*b*]indoles, see: Wenkert, E.; Alonso, M. E.; Gottlieb, H. E.; Sanchez, E. L. *J. Org. Chem.* **1977**, *42*, 3945–3949. (c) Ikeda, M.; Matsugashita, S.; Yukawa, C.; Yakura, T. *Heterocycles* **1998**, *49*, 121–126.

TABLE 1. Product Ratios of Ketene *O*,*O*-Acetals 2a−e

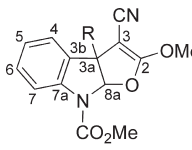

2a-e

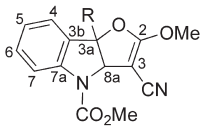

4a-e

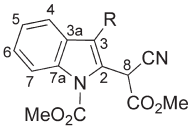

5a-e

R: **a** = Me, **b** = Et, **c** = Bn, **d** = *i*-Pr, **e** = *t*-Bu

entry	substrate	R	products[a] **2**/**4**/**5**	yield[b] (%) of **2** + **4** + **5**
1	**1a**	Me	2:1:traces	> 99
2	**1b**	Et	7:1:0	> 99
4	**1c**	Bn	9:1:0	> 99
3	**1d**	*i*-Pr	1:0:0	> 99
5	**1e**	*t*-Bu	1:0:0	> 99

[a]Determined by ^{1}H NMR (300 MHz) in acetone-d_6. [b]Overall yield based on starting **1**.

Ketene *O*,*O*-acetal **2e**, carrying a sterically bulky *t*-Bu group, was shelf-stable for at least several weeks, evidencing that this dramatic difference in the stability of the ketene *O*,*O*-acetals **2a**−**e** is tuned by the bulkiness of the alkyl substituent at the C3a bridgehead carbon, with **2a** and **2b** being much less stable entities than **2c**−**e**. Therefore, the previously described molecular ion peak $[M]^+$ shifted by 14 Da in the GC/MS spectra is attributed to the corresponding 2-indolylcyanomalonates **5a**−**e** arising from the rearrangement of ketene *O*,*O*-acetals **2a**−**e** in the column.[16] Table 1 summarizes the **2**/**4**/**5** product ratios arising from ^{1}H NMR measurements run immediately after evaporation of the reaction solvent at room temperature under atmospheric pressure with a stream of argon.

Structural Characterization of Isomeric Scaffolds 2, 4, and 5. In addition to standard ^{1}H and ^{13}C{^{1}H} NMR spectra (Figure S1−S25 in the Supporting Information), the structures of the three isomeric scaffolds **2**, **4**, and **5** were confirmed using HMBC and HSQC NMR experiments.[17] Final confirmation of the structure of **2e** was obtained from single-crystal X-ray analysis (Figure S28, Supporting Information).[18] The characteristic signals in the NMR spectra of **2a**−**e** show the bridgehead methine proton neighboring to the heteroatoms as a sharp singlet at ca. δ 6.6 ppm and a signal around δ 96−101 ppm ($^1J_{CH}$ = 180 Hz) for the corresponding bridgehead CH carbon in the ^{1}H and ^{13}C NMR spectra, respectively. In addition, the ^{13}C NMR spectra of **2a**−**e** show the alkyl-substituted quaternary carbon at ca. δ 55−66 ppm. A remarkable characteristic in this series, is the large ^{13}C chemical shift difference between the two ethylenic carbon atoms C2═C3, within a range of 106 ± 4 ppm, reflecting a significant zwitterionic character arising from their π-conjugated push−pull nature.[12,19]

The regioisomeric ketene *O*,*O*-acetals **4a**−**e** contain a typical sharp singlet around δ 5.5−5.7 ppm for the bridgehead CH proton and a signal around δ 67−70 ppm ($^1J_{CH}$ ca. 160 Hz) for the CH carbon in the ^{1}H and ^{13}C NMR spectra, respectively. Also characteristic is the ^{13}C NMR signal at δ ca. 95−102 ppm ascribed to the bridgehead quaternary carbon. On the other hand, indolylcyanomalonates **5a**−**e** could also be characterized by means of indicative NMR peaks. In particular, the methine group shows signals around δ 6.0−6.3 (singlet) and 38 ppm ($^1J_{CH}$ ca. 127 Hz) in the ^{1}H and ^{13}C NMR spectra, respectively. The sp^2 hybridation of the alkyl substituted C3 carbon is indicated by its absorbance at ca. δ 125−133 ppm in the ^{13}C NMR spectrum.[20] In this way, the ^{1}H NMR spectrum provides a simpler means to distinguish between isomeric products **2**, **4**, and **5** by comparing the chemical shift of the CH methine proton singlet signal present in all the rearranged products (Table 1).

Mechanistic Rationale for Indolylcyanomalonation by Diazomethane. From the ^{1}H results, and assuming that furo[3,2-*b*]indoles **4** are formed through rearrangement of a kinetically significant intermediate, a possible stepwise mechanism can be derived for indolylcyanomalonation by diazomethane, under thermodynamic conditions. The essential elements are shown in Scheme 1. In the first step, *O*-methylation of the enolate anion of the α-cyano-γ-lactones **1a**−**e** occurs, followed by a 1,3-shift of C−8a with the consequent ring cleavage by breaking the endocyclic C−O bond, to generate the intermediates **3a**−**e** for which the structure of a ring-contracted cyclopropane is suggested. Note that the rearrangement proceeds regioselectively; that is, the corresponding lactone arising by breaking the exocyclic C−O bond is not detected. A higher migrating aptitude of carbamate substituted methine group versus methyl group and conformational grounds can be more favorable for the methine 1,3-shift to be performed. In the second step, the driving force is probably the release of ring strain of the cyclopropane ring[21] via parallel processes, reversible ring−expansion rearrangements or ring−opening reaction, allowing either equilibration between the regioisomeric α-cyano ketene *O*,*O*-acetals **2a**−**e** and **4a**−**e** or affording the aromatized 2-indolylcyanomalonates **5a**−**e** by cleavage of the more substituted cyclopropyl bond. This latter process is therefore expected to be exothermic and irreversible, allowing the termination product in the cascade reactions.

Although at this point the formation of the key intermediate **3** could not be detected by NMR, an unambiguous proof of its structure was subsequently obtained by an X-ray crystallographic analysis of the corresponding cyclopropane **3c** (Figure 2). The structure of **3c** indicated the exo stereochemistry of the ester group. Unfortunately, all attempts to reproduce the conditions under this kinetically significant intermediate accumulates and has much longer rearrangement lifetime were unrewarding.[21] The presence of two geminally placed electron withdrawing groups at the cyclopropane ring are likely to contribute to its vulnerability in solution. It should be noted that the endocyclic cyclopropane C−C bonds of **3c** show a high level of substituent-induced bond-length asymmetry[22] with the

(16) The GC/MS of pure compounds **2e**, **4e**, and **5e** provided identical retention times and mass spectral patterns.

(17) Compounds **2a**, **2b**, **4a**, and **4b**, according to their instability, could not be isolated at the pure state.

(18) Supporting Information; see the paragraph at the end of this paper regarding availability.

(19) The substantial lower stability of α-CN ketene acetals compared with those α-CO_2Me substituted is consistent with their stronger push−pull effect. For α-CO_2Me ketene acetals $\Delta\delta$ $^{13}C_{C2=C3}$ is 84−86 ppm; see ref 12.

(20) Morales-Ríos, M. S.; Espiñeira, J.; Joseph-Nathan, P. *Magn. Reson. Chem.* **1987**, *25*, 377–395.

(21) Parker, V. D. *Pure Appl. Chem.* **2005**, *77*, 1823–1833.

(22) (a) Danishefsky, S. *Acc. Chem. Res.* **1979**, *12*, 66–72. (b) Gibe, R.; Kerr, M. A. *J. Org. Chem.* **2002**, *67*, 6247–6249. (c) Ikeda, M.; Matsugashita, S.; Tamura, Y. *J. Chem. Soc. Perkin I* **1977**, 1770–1772. (d) Alonso, M. E.; Gómez, M.; de Sierraalta, S. P.; Jano, S. P. *J. Heterocycl. Chem.* **1982**, *19*, 369–371.

SCHEME 1. Proposed Mechanism for the Cascade [1,3]-Rearrangements of 2a−e

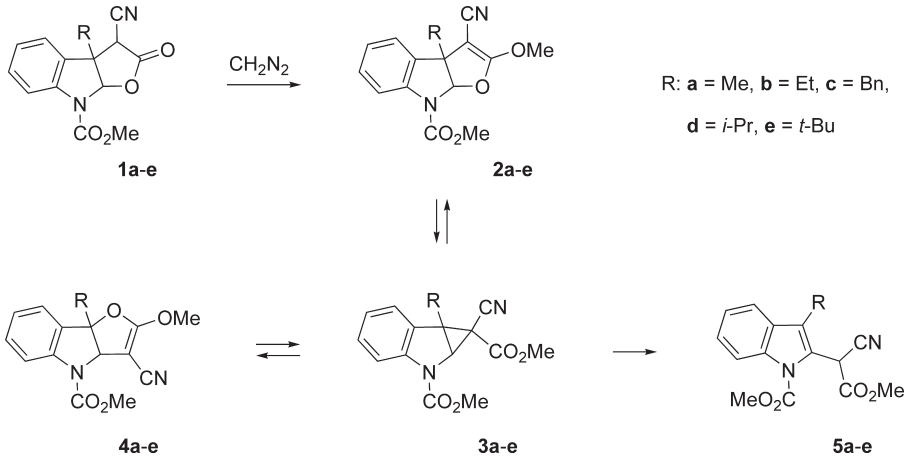

C3−C3a bond significantly elongated, as long as 1.584(3) Å, in contrast to 1.540(3) Å) and 1.487(2) Å) of the other two bonds. Thus, the high instability of intermediates **3** could be attributed, at least in part, to this long[23] and therefore weak C3−C3a bond.

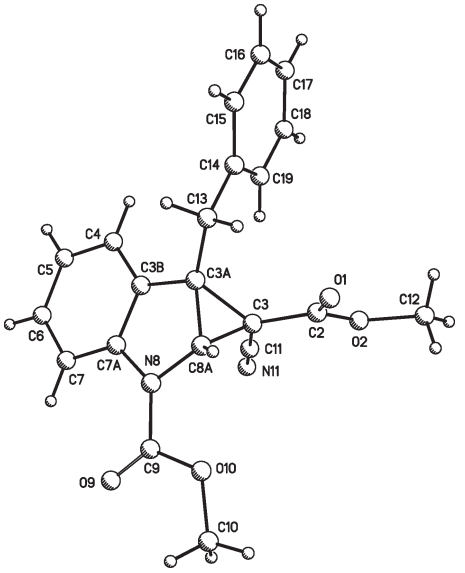

FIGURE 2. X-ray crystal structure of **3c**.

Kinetic Studies for 2a−e. Unlike the aforementioned NMR experiments of ketene *O*,*O*-acetals **2a−e** conducted in acetone-d_6, in which the reaction progress is roughly comparable to that occurring when they are stored neat, in the more polar DMSO-d_6 solvent the reaction kinetics are greatly enhanced, allowing the conversion of **2a−e** to 2-indolylcyanomalonates **5a−e** in an interval from half an hour until few weeks. The strong rate dependence for these rearrangements on the polarity of the surrounding medium may be attributed to transition states more polar than the reactants and, as such, zwitterionic processes or asynchronous bond reorganizations could conjectured to occur.[24] Kinetic and DFT level computational studies were used to discern between the aforementioned reaction mechanisms (vide infra). In general, a negligible effect on the NMR chemical shift was observed for the diagnostic CH methine signal on solvent change from acetone-d_6 to H-bond acceptor DMSO-d_6, except in the case of **5a−d** in which intermolecular hydrogen bond interactions induce a methine proton shift of ca. 0.3 ppm to higher frequency. Thus, ^{1}H NMR was used for kinetic studies, allowing direct registration of three species, a situation that is challenging. Reactions were investigated at substrate concentrations varying from 0.03 to 0.04 mmol/mL of solvent at normal probe temperature (22 °C).

We found that the rearrangement of **2a** (R = Me) in DMSO-d_6 affords **5a** in quantitative yield after only ca. 30 min reaction time (Table 2, entries 1−6), whereas the NMR-monitored experiment of the sterically more demanding **2b** (R = Et), immediately taken upon dissolution in DMSO-d_6, clearly indicated three sets of signals which represent starting **2b**, the inverted ring-fusion furo[3,2-*b*]indole **4b**, and the final rearranged product **5b**. The sharp singlet signals at δ 6.57, 5.54, and 6.28 ppm owing to the methine protons in **2b**, **4b**, and **5b**, correspondingly, had emerged in a ca. 8:1:1 ratio (Table 2, entry 7). With time, the characteristic singlet signals corresponding to **2b** and **4b** were diminishing and disappeared within 3−4 h, whereas the singlet signal assigned to **5b** (δ 6.28 ppm) steadily increased in magnitude over time and no byproducts were detected. Similar behavior is observed with the remaining ketene *O*,*O*-acetals **2c−e**. Nonetheless, on increasing the steric bulkiness of the alkyl substituent, the rate for the rearrangements decrease significantly. The ^{1}H NMR (DMSO-d_6) analysis at differing degrees of conversion of **2a−e** are summarized in Table 2. Typically, 30 min to 76 h were required to achieve ca. 90% conversion of ketene *O*,*O*-acetals **2a−e**.

From a kinetic standpoint, a steady-state approach[25] applied to kinetically significant intermediate **3** was used for the treatment of the kinetic data given in Table 2 (eq 1)

$$\mathbf{2a-e} \underset{k_{-1}}{\overset{k_1}{\rightleftharpoons}} \mathbf{4a-e} \xrightarrow{k_2} \mathbf{5a-e} \qquad (1)$$

where k_1, k_{-1}, and k_2 are the corresponding kinetic constants. However, since the reverse reaction of **4a−e** to **2a−e**

(23) Kiyohara, S.; Ishizuka, K.; Wakabayashi, H.; Miyamae, H.; Kanazumi, M.; Kato, T.; Kobayashi, K. *Tetrahedron Lett.* **2007**, *48*, 6877–6880.

(24) Reichardt, C. *Solvent Effects in Organic Chemistry*, 3rd ed.; Wiley-VCH: Weinheim, Germany, 2003.

(25) Hammett, L. P. In *Physical Organic Chemistry*, 2nd ed.; McGraw-Hill: New York, 1970; Chapter 5.

TABLE 2. Cascade Reactions Evolution[a,b] of Ketene *O*,*O*-Acetals 2a−e: Influence of the Alkyl Substituent

entry	compd	R	time (h)	mol fraction **2**:**4**:**5**	entry	compd	R	time (h)	mol fraction **2**:**4**:**5**
1	**2a**	Me	0.00	0.52:0.25:0.23	16	**2c**	Bn	3.00	0.20:0.19:0.61
2	**2a**	Me	0.03	0.45:0.23:0.32	17	**2c**	Bn	4.00	0.14:0.14:0.72
3	**2a**	Me	0.10	0.35:0.19:0.46	18	**2c**	Bn	5.00	0.11:0.11:0.78
4	**2a**	Me	0.20	0.23:0.14:0.63	19	**2d**	*i*-Pr	0.00	0.94:0.06:0.00
5	**2a**	Me	0.30	0.16:0.11:0.73	20	**2d**	*i*-Pr	3.00	0.56:0.26:0.18
6	**2a**	Me	0.50	0.08:0.06:0.86	21	**2d**	*i*-Pr	6.00	0.34:0.25:0.41
7	**2b**	Et	0.00	0.79:0.09:0.12	22	**2d**	*i*-Pr	9.00	0.20:0.16:0.64
8	**2b**	Et	0.40	0.47:0.27:0.26	23	**2d**	*i*-Pr	12.00	0.11:0.11:0.78
9	**2b**	Et	0.53	0.31:0.27:0.42	24	**2d**	*i*-Pr	15.00	0.06:0.07:0.87
10	**2b**	Et	1.33	0.20:0.21:0.59	25	**2e**	*t*-Bu	0.00	1.00:0.00:0.00
11	**2b**	Et	2.00	0.13:0.15:0.72	26	**2e**	*t*-Bu	10.00	0.69:0.27:0.04
12	**2b**	Et	2.40	0.10:0.10:0.80	27	**2e**	*t*-Bu	20.00	0.49:0.45:0.06
13	**2c**	Bn	0.00	0.86:0.10:0.04	28	**2e**	*t*-Bu	40.00	0.25:0.58:0.17
14	**2c**	Bn	1.00	0.47:0.31:0.22	29	**2e**	*t*-Bu	60.00	0.15:0.57:0.28
15	**2c**	Bn	2.00	0.30:0.26:0.44	30	**2e**	*t*-Bu	76.00	0.11:0.52:0.37

[a]Monitored by ^{1}H NMR in DMSO-d_6 solution at 22 °C. [b]Quantification of the product mixtures was followed via integration relative to residual solvent peaks from DMSO-d_6.

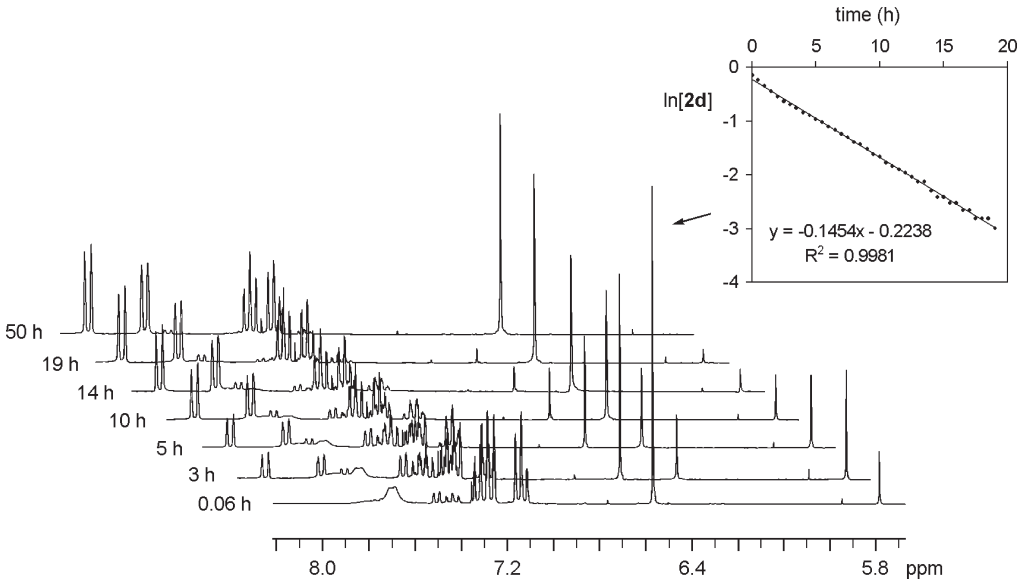

FIGURE 3. Time-dependent partial ^{1}H NMR spectra (DMSO-d_6) following the rearrangement of **2d** to **5d** at 22 °C. For the molar fraction, see Table 2. The inset shows a logarithmic curve fit of the peak height at 6.56 ppm vs time.

(k_{-1}) was inferred to be much slower than its rearrangement **2a**−**e** to **4a**−**e** (k_1),[26] the minimal kinetic model given in eq 2 may be considered and accounts for a first-order rate law expression for the disappearance of **2a**−**e** with time (eq 2).

$$\mathbf{2a{-}e} \xrightarrow{k_1} \mathbf{4a{-}e} \xrightarrow{k_2} \mathbf{5a{-}e} \qquad (2)$$

Since the transformation of **2d** or **2e** occurred slowly or very slowly (Table 2), one can assume that any of the intermediates **4d** or **4e** can be isolated from the reaction mixture, allowing the condition $k_1 \gg k_{-1}$ to be verified (vide infra). First-order rate constants were measured in duplicate runs by monitoring the disappearance of **2a**−**e** at 22 °C. As expected, plots of ln [**2**] versus time gave, in all cases, straight lines with slop k_1 (see the Supporting Information). The kinetic data are summarized in Table 3.

Typical series of NMR spectra following the rearrangement of **2d** (R = *i*-Pr) using the change in relative intensity of the methine signals are shown in Figure 3. As one can see, during the rearrangement of **2d** the ^{1}H NMR methine signal corresponding to intermediate **4d** initially grows in intensity reaching the maximum level (28%) after 3 h and then disappears gradually, with formation of indole **5d**. The intermediate cyclopropane **3d** remains at first glance undetectable during the reaction course, and no other species were observed up to 3 half-lives. The steady-state kinetic approach shows that the rate-limiting is the formation of **4d** (k_1), followed by its faster interconversion to product **5d** (k_2) (eq 2: $k_2 > k_1$).

TABLE 3. Kinetic Data (22 °C) for the Rearrangements of 2a−e[a]

compd	rate constant k_1 x 10^4 s^{-1}	half-life $t_{1/2}$/min	fit parameter R^2
2a	10.30 (±0.3)	11.2	0.998
2b	2.37 (±0.04)	48.7	0.990
2c	1.31 (±0.003)	88.2	0.995
2d	0.45 (±0.04)	259.6	0.997
2e	0.09 (±0.001)	1283.3	0.995

[a]Determined in the conversion range listed in Table 2.

(26) Because C3−C8a bond breaking in **3a**−**e** is expected to be disfavored in comparison to C3−C3a bond breaking, the ring-contraction **2a**−**e** to **3a**−**e** should be essentially irreversible on enthalpic grounds.

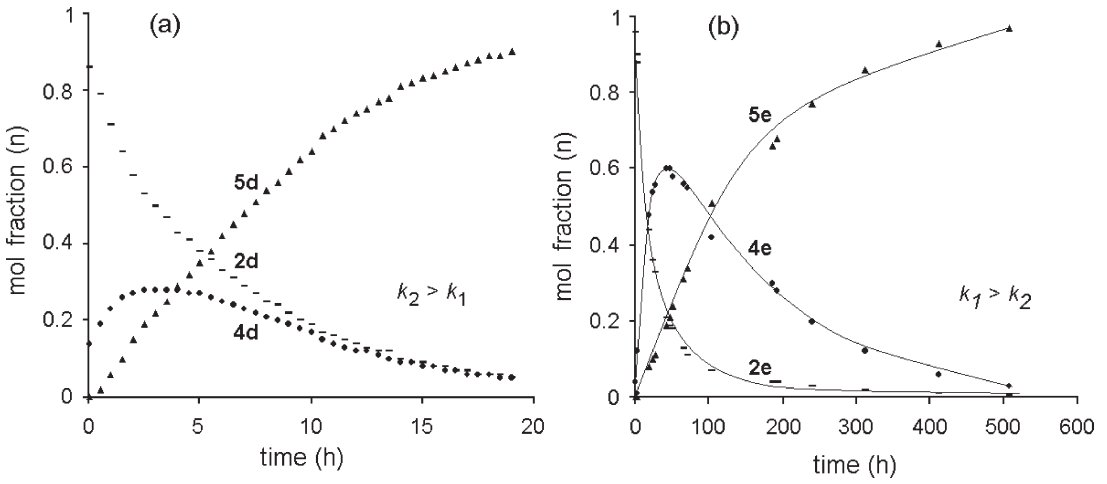

FIGURE 4. Time-dependence curves for the cascade rearrangement of (a) **2d** and (b) **2e**.

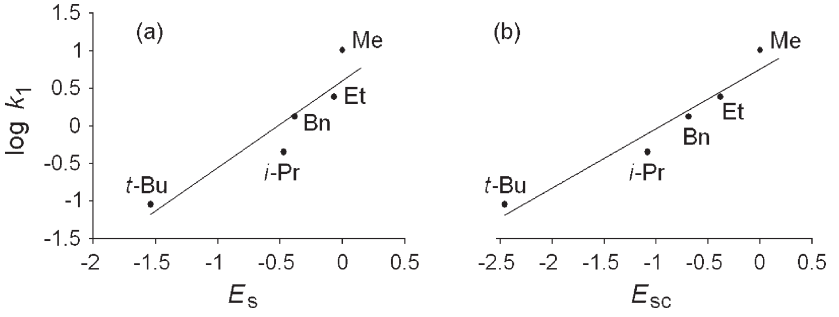

FIGURE 5. Dependence of k_1 for compounds **2a**−**e** with steric parameters: (a) E_s, (b) E_{sc}.

Examination of the kinetic data for the rearrangement of **2e** indicated a dramatic "slowing-down effect" for the bulkier *t*-Bu group, with k_1 decreasing more than 2 log units compared to the consumption of **2a** (Table 3). The time dependence curves for the cascade rearrangement of **2e** showed that, after about 2 days, the starting material **2e** achieved 80% conversion (Table 2, entries 28/29), fitting a first-order kinetics, while at the same time intermediate **4e** reached its maximum intensity value of 60%. These data evidence a change in the rate-determining step with $k_1 > k_2$ (Figure 4).

Steric Effects of the R Group. One of the main goals of this work was to quantify the steric effects of the group R on the reactivity of ketene *O*,*O*-acetals **2a**−**e**. Thus, the reaction kinetics were analyzed as function of the substitution degree on the carbon directly bounded to the ketene acetal group, comprising primary R groups (Me and Et), secondary (benzyl and isopropyl), as well as tertiary ones (tertbutyl). Figure 6 shows the correlations found between the rate constants (k_1) of disappearance of substrates **2a**−**e** with time and the steric substituent parameter E_s originated by Taft[27] and its correction E_{sc}[28] (Table 4). We observed that the curve for k_1 as function of E_s does not show a good correlation ($R^2 = 0.844$). However, a highly significant improvement in fit was obtained when the steric parameter E_{sc} was applied

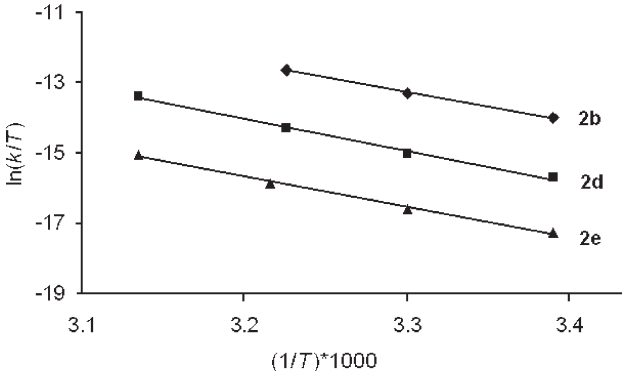

FIGURE 6. Eyring plots for the rearrangements of **2b**, **2d**, and **2e**.

($R^2 = 0.932$, slope = 0.788), confirming that the steric bulkiness of the R group is the main factor determining the observed kinetic trend in these rearrangements. Clearly, the rate constant (k_1) for **2e** (R = *t*-Bu) exceeds in relation to the corresponding steric parameter E_{sc} (Figure 5b), as predicted by a line passing through the points for the first four compounds ($R^2 = 0.983$, slope = 1.226). The interpretation of this fact in terms of the transition state is that the bulky *t*-Bu group could cause a relative enthalpically based steric acceleration by bond lengthening. Considering the fact that the k_1 rates for these rearrangements decrease linearly in the order of increasing steric effect E_{sc} (Table 4), then it can be argued that bulky substituents at C3a destabilize the transition states more than they destabilize the starting materials.

(27) (a) Pavelich, W. A.; Taft, R. W. *J. Am. Chem. Soc.* **1957**, *79*, 4935–4940. (b) Unger, S. H.; Hansch, C. In *Progress in Physical Organic Chemistry*; Taft, R. W., Ed.; John Wiley and Sons: New York, 1976; Vol. 12, pp 91−118.

(28) Hancock, C. K.; Meyers, E. A.; Yager, B. J. *J. Am. Chem. Soc.* **1961**, *83*, 4211.

TABLE 4. Steric Substituent Parameters for R Groups

R	E_s[27]	E_{sc}[28]
Me	0.00	0.00
Et	−0.07	−0.38
Bn	−0.38	−0.69
isopropyl	−0.47	−1.08
tertbutyl	−1.54	−2.46

TABLE 5. Activation Parameters for the Rearrangements of 2b, 2d, and 2e

compd	$\Delta H^{\ddagger}$ (kcal mol^{-1})	$\Delta S^{\ddagger}$ (cal K^{-1} mol^{-1})	$\Delta G^{\ddagger}_{(298)}$ (kcal mol^{-1})
2b	20.78	−17.66	22.22
2d	22.28	−16.90	23.21
2e	21.18	−23.03	24.14

Thermodynamic Parameters of the Transition State for 2b, 2d, and 2e. With the aim of determining the enthalpic ($\Delta H^{\ddagger}$) and entropic ($\Delta S^{\ddagger}$) components of the steric effects for transition states reached from reactants **2b**, **2d**, and **2e**, the effect of temperature on reaction rates was studied at three different temperatures over the range of 22−37 °C for the disappearance of **2b** and at four different temperatures from 22 to 46 °C for the disappearance of **2d** and **2e** in DMSO-d_6. Because the precision of the NMR data and the narrow temperature range in which these rearrangements could be conveniently studied, the corresponding values $\Delta H^{\ddagger}$ and $\Delta S^{\ddagger}$ are probably reliable to ±1 kcal mol^{-1} and 2−3 eu, respectively. The first-order rate of these reactions was determined by repeating the reactions two times at each of the chosen temperatures (see the Supporting Information), and the activation parameter values calculated from Eyring plots are displayed in Table 5. In all cases studied, good linear correlations of ln (k/T) versus $1/T$ were obtained (Figure 6), indicating that the calculated activation parameters depend only on the nature of the rearrangement process. The low activation energies and the strongly negative entropies of activation, in the range associated with unimolecular processes,[29] provide evidence for a concerted [1,3]-sigmatropic rearrangement via a four-membered pseudopericyclic transition state[30] and, therefore, with loss in conformational freedom. The large negative entropy values can also imply that the polar environment stabilizes the transition states (**TS**) more than the ground state (**GS**) as solvation is more efficient, with a lower rearrangement energy barrier. The observed enthalpic activation trend in the order **2d** > **2e** > **2b** (Table 5) is consistent with our preceding proposal that rearrangement of **2e** proceeds with a relative enthalpically based steric acceleration of the tertbutyl group. In addition, we expected entropy loss upon forming the transition state to be lower with bulkier substituents, because of hindered motion in the **GS**, and in fact, this is the observed trend between **2b** and **2d**. However, the entropy parameter for **2e** is 5.4 or 6.1 cal K^{-1} mol^{-1} lower than that of **2b** or **2d**, respectively. We attributed the increase in negative entropy of activation for the rearrangement of **2e** to destabilizing effects of the sterically bulky *t*-Bu group in achieving a specific conformation in which the four-membered transition state can occur.

TABLE 6. Kinetic Data (22 °C) for the Rearrangements of 4d and 4e

compd	rate constant k_2 x 10^4 s^{-1}	half-life $t_{1/2}$/min	fit parameter R^2
4d	0.74 ± 0.09	152	0.996
4e	0.02[a]	5391	0.996

[a]Single run.

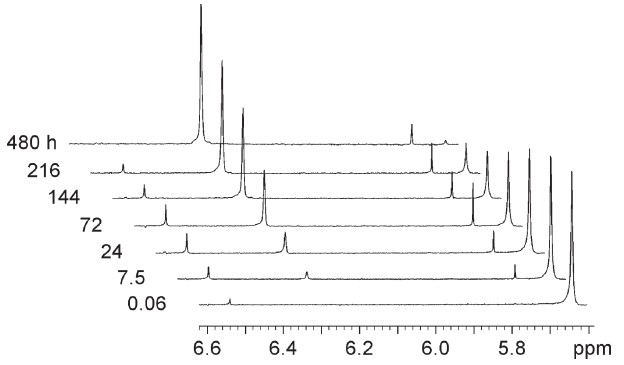

FIGURE 7. Time-dependent partial ^{1}H NMR spectra (DMSO-d_6) following the rearrangement of **4e**.

Kinetic Studies for 4d and 4e. In light of the above results, and to support the mechanistic details for the cascade rearrangements of **2a**−**e** (Scheme 1), we attempted to isolate regioisomeric indolines **4**. Representative **4d** and **4e** were successfully isolated in 27% and 58% yield, respectively (see the Experimental Section) and characterized on the basis of their NMR spectral data. An unambiguous proof of the structure of the inverted ring-fusion furo[3,2-*b*]indoles **4d** and **4e** was established by their crystal structure analysis[31] (Figures S30 and S31, Supporting Information).

When a DMSO-d_6 solution of **4d** was monitored by NMR spectroscopy at 22 °C, a clean first-order rearrangement to **5d** was observed as far as the reaction proceeds to a 90% conversion (~8.5 h) (Table 6). As expected from the curve-fittings in Figure 4, the transformation of **4d** to **5d** (k_2) took place faster than that of **2d** to **4d** (k_1). Thus, **2d**→**4d** was the rate-determining step of the overall reaction.

The most fully defined outcome in these kinetic studies was obtained by monitoring the rearrangement of the furo-[3,2-*b*]indole **4e** (Table 6) by taking the ^{1}H NMR spectra over a period of approximate 20 days at normal probe temperature (22 °C). Typical series of NMR spectra following the rearrangement of **4e** using the change in relative intensity of the methine signals are shown in Figure 7. As can be seen, the NMR spectrum of **4e** obtained after 7.5 h reaction time showed, in addition to the expected single signals attributable to each of the methine protons of starting furo[3,2-*b*]indole **4e** (δ 5.64) and the final rearranged product **5e** (δ 6.28), two clean sharp singlets at δ 6.54 and δ 5.73 ppm whose height remains less than 8% and almost constant through the rearrangement process. The singlet signal at δ 6.54 ppm corresponds to furo[2,3-*b*]indole **2e** and, therefore, does not exert a significant influence on the overall rate, setting

(29) (a) Bates, G. S.; Ramaswamy, S. *Can. J. Chem.* **1981**, *59*, 3120–3122. (b) Frey, H. M.; Solly, R. K. *Trans. Faraday Soc.* **1968**, *64*, 1858.

(30) (a) Jones, G. O.; Li, X.; Hayden, A. E.; Houk, K. N.; Danishefsky, S. J. *Org. Lett.* **2008**, *10*, 4093–4096. (b) Çelebi-Ölçüm, N.; Aviyente, V.; Houk, K. N. *J. Org. Chem.* **2009**, *74*, 6944–6952.

(31) A significant shortening of the C3−C11 bond in **4d** (1.407(3) Å) and **4e** (1.405(3) Å) as compared to the C3−C11 bond in **3c** (1.442(3) Å) was observed.

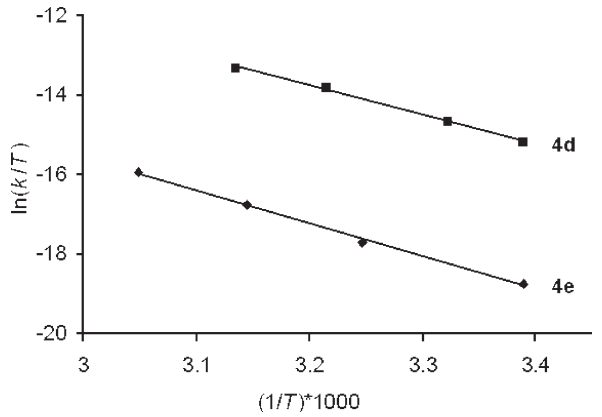

FIGURE 8. Eyring plots for the rearrangements of **4d** and **4e**.

TABLE 7. Activation Parameters for the Rearrangements of 4d and 4e

compd	$\Delta H^{\ddagger}$ (kcal mol^{-1})	$\Delta S^{\ddagger}$ (cal K^{-1} mol^{-1})	$\Delta G^{\ddagger}_{(298)}$ (kcal mol^{-1})
4d	18.01	−27.56	22.90
4e	20.15	−28.8	25.03

$k_1 \gg k_{-1}$. The new singlet at δ 5.73 ppm was associated with the methine group of the kinetically significant intermediate **3e**. The peak at δ 5.64 ppm nearly disappeared over a period of 20 days, indicating the decay of starting **4e**. The height of peak at δ 6.28 ppm increased over the same time period, evidencing the formation of **5e**. Hence, we conclude Scheme 1 shows the correct mechanism of cascade rearrangements. The collected NMR data fitted to a first-order rate law over three half-life periods supporting the validity of the steade-state kinetic approach used for data interpretation (eq 2). Comparison between k_1 and k_2 showed that the product rate formation, **4e** → **5e** step (k_2), is slower than the rate decay of the substrate, **2e** → **4e** step (k_1).Therefore, in this two-step consecutive unimolecular model, the rate-determining step is the formation of **5e**.

Thermodynamic Parameters of the Transition State for 4d and 4e. Figure 8 shows k_2 values for the disappearance of regioisomeric indolines **4d** and **4e** in DMSO-d_6 at four different temperatures over the range of 22−46 °C for **4d** and of 22−55 °C for **4e** plotted according to the Eyring equation (see the Supporting Information). The activation parameters are listed in Table 7.

Temperature-dependent rate studies demonstrate substantial negative entropies of activation for the rearrangements of **4d** and **4e** (Table 7), which may be indicative of concerted unimolecular processes with highly ordered transition states. The entropic cost of **4d** or **4e** is balanced in its contribution to the free energy of activation ($\Delta G^{\ddagger}$) by an enthalpic benefit as compared to **2d** or **2e** (Table 5), respectively. In agreement with the rate-determining step, k_1 for R = *i*-Pr or k_2 for R = *t*-Bu (vide supra), it was found that the difference in free energy between transition states reached from **2d** and **4d** is lower for **4d** ($\Delta\Delta G^{\ddagger} = 0.31$ kcal mol^{-1}; $k_2 > k_1$), while this difference between **2e** and **4e** is lower for **2e** ($\Delta\Delta G^{\ddagger} = 0.89$ kcal mol^{-1}; $k_1 > k_2$).

Computational Considerations on the 1,3-Shifts. In conjunction with kinetic studies, which provided evidence suggesting that rearrangements of ketene *O*,*O*-acetals **2a**−**e** occur via a concerted mechanism, we have modeled the rearrangement of computationally less expensive substrate **2a** in an attempt to increase our understanding on these fundamental rearrangements and in fact to confirm or invalidate the postulated mechanism based on an energetically reasonable pathway.

An initial systematic conformational search was performed for the reactant, intermediates, and product at the B3LYP/6-31G(d) theoretical level[32] using Spartan 04[33] and then optimized at the same level of theory using Gaussian 03 suite of quantum chemical programs. Geometry optimizations of transition states (**TS**), as well as concerted or stepwise pathways for the 1,3-rearrangements were also explored at the B3LYP/6-31G(d) theoretical level using Gaussian 03.[34] Structures at stationary points were characterized by frequency analysis and reported energies include zero-point energy (ZPE) corrections scaled by 0.9806.[35] Solvent effects were taken into account via geometry optimization and frequency calculations using a polarized continuum model (PCM)[36] in DMSO as the solvent. The free energy (G) of a given structure in the solvent was calculated by eq 3.

$$G = E_{\text{gas}} + E_{\text{zpe + thermal}} \tag{3}$$

where E_{gas} is the gas-phase electronic energy and $E_{\text{zpe+thermal}}$ is the sum of the zero-point energy and the thermal free energy contributions to the gas-phase energy at 298.15 K.

The optimized geometries of substrate **2a** and intermediates **3a** and **4a** evidence the remarkable rigidity of these molecular structures, which show only two stable conformers having the carbonyl carbamate group *syn* and *anti* to the H7 benzene ring proton, respectively. The *syn* conformation is the most stable in the gas phase by 1.1−2.8 kcal mol^{-1} (Supporting Information) and was the only one considered toward the construction of reaction profiles. These results are summarized in Figure 9. It should be noted that the *syn* conformation was observed in all of the X-ray crystal structures of related compounds (**2e**, **3c**, **4d**, and **4e**).

The next step in our study was to analyze both the stepwise and concerted processes. In all of our attempts to find the reaction pathway involving ionic intermediates, we observed that the concerted shift occurred before a stable ionic

(32) (a) Becke, A. D. *J. Chem. Phys.* **1993**, *98*, 5648–5652. (b) Becke, A. D. *J. Chem. Phys.* **1993**, *98*, 1372–1377. (c) Lee, C.; Yang, W.; Parr, R. G. *Phys. Rev. B* **1988**, *37*, 785–789. (d) Stephens, P. J.; Devlin, F. J.; Chabalowski, C. F.; Frisch, M. J. *J. Phys. Chem.* **1994**, *98*, 11623–11627.

(33) *Spartan 04 Wavefunction*, Irvine, CA, 2004.

(34) *Gaussian03*, (Revision C.02): Frisch, M. J.; Trucks, G. W.; Schlegel, H. B.; Scuseria, G. E.; Robb, M. A.; Cheeseman, J. R.; Montgomery, J. A., Jr.; Vreven, T.; Kudin, K. N.; Burant, J. C.; Millam, J. M.; Iyengar, S. S.; Tomasi, J.; Barone, V.; Mennucci, B.; Cossi, M.; Scalmani, G.; Rega, N.; Pettersson, G. A.; Nakatsuji, H.; Hada, M.; Ehara, M.; Toyota, K.; Fukuda, R.; Hasegawa, J.; Ishida, M.; Nakajima, T.; Honda, Y.; Kitao, O.; Nakai, H.; Klene, M.; Li, X.; Knox, J. E.; Hratchian, H. P.; Cross, J. B.; Bakken, V.; Adamo, C.; Jaramillo, J.; Gomperts, R.; Stratmann, R. E.; Yazyev, O.; Austin, A. J.; Cammi, R.; Pomelli, C.; Ochterski, J. W.; Ayala, P. Y.; Morokuma, K.; Voth, G. A.; Salvador, P.; Dannenberg, J. J.; Zakrzewski, V. G.; Dapprich, S.; Daniels, A. D.; Strain, M. C.; Farkas, O.; Malick, D. K.; Rabuck, A. D.; Raghavachari, K.; Foresman, J. B.; Ortiz, J. V.; Cui, Q.; Baboul, A. G.; Clifford, S.; Cioslowski, J.; Stefanov, B. B.; Liu, G.; Liashenko, A.; Piskorz, P.; Komaromi, I.; Martin, R. L.; Fox, D. J.; Keith, T.; Al-Laham, M. A.; Peng, C. Y.; Nanayakkara, A.; Challacombe, M.; Gill, P. M. W.; Johnson, B.; Chen, W.; Wong, M. W.; Gonzalez, C.; Pople, J. A. Gaussian, Inc., 2003.

(35) Scott, A. P.; Radom, L. *J. Phys. Chem.* **1996**, *100*, 16502–16513.

(36) (a) Miertus, S.; Tomasi, J. *Chem. Phys.* **1982**, *65*, 239–245. (b) Miertus, S.; Scrocco, E.; Tomasi, J. *Chem. Phys.* **1981**, *55*, 117–129.

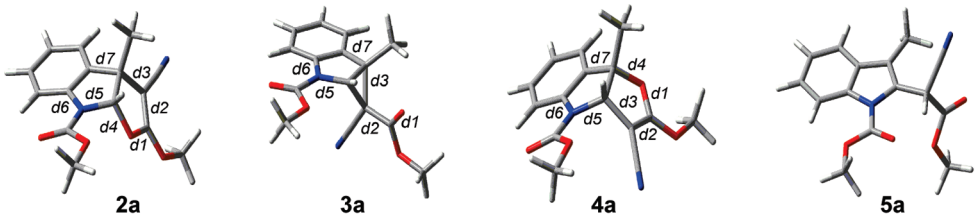

0.0 (0.0) -2.5 (-3.8) -3.0 (-3.3) -17.1

	*d*1 (Å)	*d*2 (Å)	*d*3 (Å)	*d*4 (Å)	*d*5 (Å)	*d*6 (Å)	*d*7 (Å)	μ (Debyes)
2a$_{gas}$	1.347	1.363	1.532	1.456	1.445	1.422	1.523	3.02
2a$_{DMSO}$	1.345	1.366	1.534	1.460	1.447	1.422	1.522	3.91
3a$_{gas}$	1.217	1.499	1.591	-	1.436	1.416	1.496	3.69
3a$_{DMSO}$	1.218	1.499	1.596	-	1.437	1.418	1.496	4.96
4a$_{gas}$	1.341	1.363	1.512	1.485	1.487	1.406	1.505	6.13
4a$_{DMSO}$	1.332	1.369	1.512	1.490	1.489	1.410	1.505	8.88

FIGURE 9. Low energy conformers of **2a**−**4a** (gas phase), relative energies (kcal mol^{-1}), ΔG_{gas} (ΔG_{DMSO}), selected bond lengths (*d*, Å), dipole moments (μ, debyes), and the optimized structure of indole **5a** (gas phase).

TABLE 8. Activation Free Energies $\Delta G^{\ddagger}_{gas\ phase}$ and $\Delta G^{\ddagger}_{DMSO}$ (in kcal mol^{-1}) for the [1,3] Rearrangements of 2a and 4a[a]

	$\Delta G^{\ddagger}_{gas\ phase}$	$\Delta G^{\ddagger}_{DMSO}$
2a→**TS1**→**3a**	28.1 (30.6)	21.3 (25.1)
4a→**TS2**→**3a**	31.1 (30.6)	24.7 (25.2)

[a]Reverse reaction energies are given in parentheses.

transition structure was found.[37] Thus, theoretical calculations indicated that regioisomers **2a** and **4a** rearranged in one step processes to give ring contracted **3a** through planar four-membered transition states **TS1** and **TS2**, respectively. As can be seen from Table 8, the $\Delta G^{\ddagger}$ values for **TS1** and **TS2** in the gas phase are found to be higher in energy than those calculated with the incorporation of the DMSO solvent environment. Values of $\Delta G^{\ddagger}$ in DMSO phase are in the range of those determined experimentally, contributing to validate our approach. Because of the geometrical restrictions, regioisomers **2a** and **4a** are expected to rearrange via suprafacial shifts with inversion of configuration at the migrating carbon center, leading both to a highly stereoselective formation of the cyclopropane diastereomer **3a**, in which the R and cyano groups are *trans* to each other.[38] The orbital symmetry theory predicts that thermal, suprafacial 1,3-shifts with retention of configuration are forbidden.[39] However, 1,3-shifts become allowed if the migrating group possesses a p-orbital within a pseudopericyclic orbital topology,[40] as we observed. The stereochemistry of computed **3a** is in very good agreement with the X-ray structure for structurally related compound **3c**.

As can be seen from the data in DMSO phase (Table 8), the barrier for ring contraction of **2a** (21.3 kcal mol^{-1}) to yield **3a** is substantially lower than that for ring contraction of **4a** (24.7 kcal mol^{-1}) to yield **3a**. This energy difference is essentially due to the relative stability of substrates **2a** and **4a**. In this connection, we noticed that the reverting back ring contraction reaction of **4a** to yield **3a** is 0.5 kcal mol^{-1} lower in energy than the ring expansion reaction of **3a** to yield **4a**. Since the [1,3]-rearrangements are under thermodynamic control, the **TS2** presumably plays a decisive role in determining the rate-determining step. The high stability of indole **5a** could be the driven force for the reactions to occur.

Inspection of transition-state geometries for **TS1** and **TS2** were performed, and their main geometric features are shown in Figure 10. All discussion refers to DMSO solvent phase. Despite being concerted, the **2a** → **3a** and **4a** → **3a** rearrangements appears to be highly asynchronous as shown by the **TS1** and **TS2** geometries, respectively. While *d*3 distances are relatively short (2.447 or 2.524 Å) the *d*4 distances are very long (2.603 or 2.853). The largest structural changes of **TS1** with respect to fully formed bonds in **2a** are the pronounced decrease in the forming O=C bond length (*d*1 **TS1** = 1.243 Å and *d*1 **2a** = 1.345 Å) concomitant with an increase in the breaking O−C bond length (*d*4 **TS1** = 2.603 Å and *d*4 **2a** = 1.460 Å). The shortening of the N−C bond length for **TS1** as compared to **2a** (*d*5 **TS1** = 1.317 Å and *d*5 **2a** = 1.447 Å) is suggesting that the opening of the ketene acetal ring is assisted by the indole nitrogen lone pair. Similarly, for **TS2** the main structural differences with respect to **4a** are the forming O1=C2 bond length (*d*1 **TS2** = 1.236 Å and *d*1 **4a** = 1.332 Å) and the breaking O−C bond length (*d*4 **TS2** = 2.853 Å and *d*4 **4a** = 1.490 Å). In this case, a delocalization of the nitrogen lone pair through the adjacent benzene ring is operating, as clearly evidenced the shortening in the N−C and C−C bond lengths as compared to **4a** (*d*6 **TS2** = 1.368 Å and

(37) This result could indicate that the ionic path has a transition state too high in energy which crosses the surface of the sigmatropic shift, or simply does not exist.

(38) The *trans*-cyclopropane **3a** is more stable than its contrathermodynamic *cis* counterpart by 12.5 kcal mol^{-1} in the gas phase.

(39) (a) Hoffmann, R.; Woodward, R. B. *J. Am. Chem. Soc.* **1965**, *87*, 4389–4390. (b) Woodward, R. B.; Hoffmann, R. *J. Am. Chem. Soc.* **1965**, *87*, 2511–2513. (c) Pearson, R. G. *Symmetry Rules for Chemical Reactions*, 1st ed.; John Wiley and Sons: New York, 1976.

(40) (a) Ross, J. A.; Seiders, R. P.; Lemal, D. M. *J. Am. Chem. Soc.* **1976**, *98*, 4325–4327. (b) Birney, D. M.; Wagenseller, P. E. *J. Am. Chem. Soc.* **1994**, *116*, 6262–6270. (c) Birney, D. M. *J. Am. Chem. Soc.* **2000**, *122*, 10917–10925.

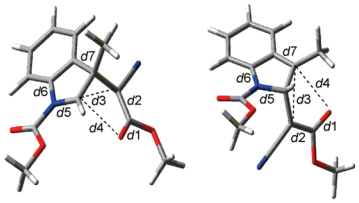

	*d*1 (Å)	*d*2 (Å)	*d*3 (Å)	*d*4 (Å)	*d*5 (Å)	*d*6 (Å)	*d*7 (Å)	μ (Debyes)
$\mathbf{TS1}_{gas}$	1.245	1.427	2.396	2.515	1.332	1.438	1.527	8.47
$\mathbf{TS1}_{DMSO}$	1.243	1.424	2.447	2.603	1.317	1.442	1.545	12.97
$\mathbf{TS2}_{gas}$	1.234	1.435	2.471	2.713	1.493	1.369	1.398	7.09
$\mathbf{TS2}_{DMSO}$	1.236	1.427	2.524	2.853	1.400	1.368	1.390	12.81

FIGURE 10. Transition-state geometries (**TS1** and **TS2**) in DMSO solvent phase, bond lengths (*d*, Å), and dipole moments (*μ*, debyes) for the [1,3]-rearrangements of **2a** and **4a**.

d6 **4a** = 1.410 Å; and *d*7 **TS2** = 1.390 Å and *d*7 **4a** = 1.505 Å). Additionally, it can be envisaged that in **TS1** and **TS2** unfavorable steric constraints developed between the O=C double bond formation and the methyl group, explaining the experimentally determined energetic penalty originated by bulkier R groups. Because of the high degree of asynchronous character of the transition states, polarization is found to be higher than in the ground states. In the "hill climb" movement from the reactants **2a** and **4a** to **TS1** and **TS2**, respectively, the dipole moment significantly increase, suggesting that considerable charge separation is involved in transition states. The dipole moments of compounds **2a** and **4a** and transition states **TS1** and **TS2** are 3.91, 8.88, 12.97, and 12.81 D, respectively (Figures 9 and 10). These computational studies forward to a fundamental understanding of the experimentally observed steric and solvent rate effects.

Conclusions

The present study constitutes a significant advancement in the mechanistic elucidation of the cascade rearrangements of indol derived α-cyano ketene *O*,*O*-acetals to afford 2-indolyl cyanomalonates in quantitative yields. On the basis of the simplified kinetic equation used for data interpretation of the kinetic results and computational studies, we propose that the transformations involve the combination of four concerted [1,3]-sigmatropic shifts, and a vicinal hydrogen transfer for the final aromatization step. A mechanistic highlight resides in the pivotal role assigned to the steady-state cyclopropyl intermediate in directing the cascade rearrangements. These processes are unique in the sense that, absent significant polar substituent effects, the reaction rate of ketene *O*, *O*-acetals decrease linearly and dramatically in the order of increase the steric effect. The observed solvent rate effects are attributable to a selective transition-state stabilization by increased polarization stabilization because of the asynchronous bond reorganization processes. Work is in progress to profit these compounds as precursors to bioactive indolic *β*-amino acids.

Experimental Section

3a-Benzyl 2-Oxofuroindoline (1c). To a cooled solution (0 °C) of BnMgBr (683.7 mg, 3.5 mmol) in Et_2O (13 mL)/THF (20 mL) under argon atmosphere was added **6** (250 mg 0.87 mmol) in a THF (10 mL) solution over a period of 30 min with stirring. The temperature was maintained at 0 °C for 3 h during which the mixture turned orange. The temperature was allowed to rise to room temperature, and the reaction mixture was quenched with saturated aqueous NH_4Cl solution (5 mL) and diluted with EtOAc (30 mL). The organic layer was decanted, washed with saturated aqueous NH_4Cl solution (2 × 10 mL), and dried (Na_2SO_4). After evaporation of the solvent under vacuum, the residue was purified by flash column chromatography (silica gel, hexane/EtOAc 6:1) to give 195 mg of **1c** (59%). Two recrystallizations from hexane/AcOEt gave a colorless solid. Mp: 157−158 °C. IR (CH_2Cl_2, cm^{-1}): ν_{max} 3026, 2256, 1734 cm^{-1}. **Endo isomer** (for 11:2 endo/exo mixture) ^1H NMR (300 MHz, $CDCl_3$): *δ* 7.85 (br, 1H, H7), 7.68 (d, 1H, *J* = 7.8 Hz, H4), 7.42 (t, 1H, *J* = 7.3 Hz, H6), 7.34 (m, 3H, Ar), 7.22 (td, 1H, *J* = 7.8, 1.0 Hz, H5), 7.04 (m, 2H, Ar), 6.38 (br, 1H, H8a), 4.15 (s, 1H, interchangeable by deuterium, H3), 3.90 (s, 3H, COOMe), 3.13 and 3.08 (2d, 2H, J_{AB} = 14.2 Hz). ^{13}C NMR (75 MHz, $CDCl_3$) *δ*: 164.7 (s, C2), 155.1 (s, NCO), 140.2 (s, C_i), 133.2 (s, C7a), 131.0 (d, C6), 129.9 (d, CO), 129.3 (d, C_m), 128.3(d, C_p), 128.0 (d, C3b), 125.7 (d, C4), 124.7 (d, C5), 115.9 (d, C7), 112.4 (s, CN), 93.7 (d, C8a), 55.2 (s, C3a), 53.7 (q, COO*Me*), 42.3 (t, CH_2), 40.5(s, C3, Me). MS (EI), *m*/*z*: (relative inensity) 348 (M^+, 100), 213 (79). HRMS (FAB), *m*/*z*: 349.1185 (M^+, $C_{20}H_{16}N_2O_4$ + H requires 349.1188). **Exo isomer**: The ^1H NMR spectrum of the minor exo isomer cannot be fully characterized due to extensive overlapped signals: *δ* 4.08 (s, 1H, interchangeable by deuterium, H3), 3.79 (s, 3H, COOMe), 3.42 and 3.29 (2d, 2H, J_{AB} = 13.7 Hz).

General Procedure for Reaction of Furoindolines 1a−e with Diazomethane. To an Et_2O (6 mL)/THF (2 mL) solution of the corresponding 3a-alkyl-2-oxofuroindoline **1a−e** (0.17 − 0.22 mmol) was added an excess of freshly prepared ethereal solution of diazomethane[13] (10 mL, ca. 5.3 mg CH_2N_2/mL, 1.3 mmol). The reaction mixture was stirred at room temperature for 5 min and evaporated at room temperature under atmospheric pressure with a stream of argon which was bubbled into a solution containing 5% acetic acid in ethanol.

Methyl 3-Cyano-2-methoxy-3a-methyl-3a*H*-furo[2,3-*b*]indole-8(8a*H*)-carboxylate (2a), Methyl 3-Cyano-2-methoxy-8b-methyl-3a*H*-furo[3,2-*b*]indole-4(8b*H*)-carboxylate (4a), and Methyl 2-(1-Cyano-2-methoxy-2-oxoethyl)-3-methyl-1*H*-indole-1-carboxylate (5a). Following the general procedure, reaction of furoindoline **1a** with diazomethane gave a colorless oil mixture of isomeric products **2a**, and **4a** in proportions of 1:1 in an overall >99% yield. This material was standing at 22 °C in DMSO (1 mL) until

its complete transformation (1 h), and then concentrated to dryness to afford the pure enough indole **5a** as colorless solid in >99% yield. Due to the reaction progress, the spectral NMR data of **2a** and **4a** listed below stem from the 2:1 mixture for ^{1}H and from the 1:2 mixture for ^{13}C.

2a. ^{1}H NMR (300 MHz, acetone-d_6): δ 7.83 (br s, 1H, H7), 7.37 (dd, J = 7.4, 1.4 Hz, H4), 7.33 (td, 1H, J = 7.4, 1.4 Hz, H6), 7.17 (td, J = 7.7, 1.1 Hz, H5), 6.56 (s, 1H, H8a), 4.05 (s, 3H, OMe), 3.93 (s, 3H, COOMe), 1.71 (s, 3H, Me). ^{13}C NMR (75 MHz, acetone-d_6): δ 170.7 (s, C2), 154.3 (s, N-CO), 141.5 (s, C7a), 137.3 (s, C3b), 130.2 (d, C6), 125.7 (d, C5), 123.9 (d, C4), 116.6 (d, C7), 116.4 (s, CN), 101.4 (d, C8a), 65.3 (s, C3), 59.5 (q, OMe), 55.1 (s, C3a), 54.4 (q, COO*Me*), 24.4 (q, Me).

4a. ^{1}H NMR (300 MHz, acetone-d_6): δ 7.94 (br s, 1H, H7), 7.57 (dd, 1H, J = 7.7, 1.4 Hz, H4), 7.46 (td, J = 7.4, 1.4 Hz, H6), 7.17 (td, J = 7.7, 1.1 Hz, H5), 5.47 (s, 1H, H8a), 4.02 (s, 3H, OMe), 3.85 (s, 3H, COOMe), 1.94 (s, 3H, Me). ^{13}C NMR (75 MHz, acetone-d_6): δ 173.4 (s, C2), 153.8 (s, N-CO), 143.7 (s, C7a), 132.8 (d, C6), 131.2 (s, C3b), 125.9 (d, C4), 124.9 (d, C5), 117.1 (s, CN), 116.7 (d, C7), 95.3 (s, C3a), 72.5 (d, C8a), 60.0 (s, C3), 59.1 (q, OMe), 53.5 (q, COO*Me*), 24.7 (q, Me).

5a. Pure sample was obtained by recrystallization from a mixture of CH_2Cl_2/hexane to give a white solid. Mp: 138−140 °C. R_f 0.39 (CH_2Cl_2). IR ($CHCl_3$) ν_{max} 3016, 2254, 1752, 1612 cm^{-1}; ^{1}H NMR (300 MHz, acetone-d_6): δ 8.19 (dt, 1H, J = 8.2, 0.9, H7), 7.68 (dd, 1H, J = 7.7, 1.5 Hz, H4), 7.46 (td, 1H, J = 7.2, 1.3 Hz, H6), 7.37 (td, 1H, J = 7.7, 1.1 Hz, H5), 6.00 (s, 1H, H8), 4.11 (s, 3H, NCOOMe), 3.84 (s, 3H, COOMe), 2.43 (s, 3H, Me). ^{13}C NMR (75 MHz, acetone-d_6): δ 166.4 (s, C*CO*), 153.1 (s, NCO), 137.2 (s, 7a), 131.2 (s, C3a), 127.5 (d, C6), 125.7 (s, C3), 125.0 (d, C5), 122.1 (s, C2), 121.1 (d, C4), 117.1 (d, C7), 116.5 (s, CN), 55.1 (q, NCOO*Me*), 54.7 (q, COO*Me*), 37.7 (d, C8), 9.5 (q, Me). MS (EI), m/z: (relative inensity) 286 (M^+, 44), 254 (100), 227 (81). HRMS (FAB), m/z: 309.0859 (M^+, $C_{15}H_{14}N_2O_4$ + Na requires 309.0851).

Methyl 3-Cyano-3a-ethyl-2-methoxy-3a*H*-furo[2,3-*b*]indole-8(8a*H*)-carboxylate (2b), Methyl 3-Cyano-8b-ethyl-2-methoxy-3a*H*-furo[3,2-*b*]indole-4(8b*H*)-carboxylate (4b), and Methyl 2-(1-Cyano-2-methoxy-2-oxoethyl)-3-ethyl-1*H*-indole-1-carboxylate (5b). Following the general procedure, reaction of furoindoline **1b** with diazomethane gave a colorless oil mixture of isomeric products **2b** and **4b** in proportions of 7:1 in an overall >99% yield. This material was standing at 22 °C in DMSO (1 mL) until its complete transformation (4 h), and then concentrated to dryness to afford pure enough indole **5b** as colorless crystals in >99% yield. Due to the reaction progress, the spectral NMR data of **2b** and **4b** listed below stem from the 2:1 mixture for ^{1}H and from the 1:1 mixture for ^{13}C.

2b. ^{1}H NMR (300 MHz, acetone-d_6): δ 7.79 (br s, 1H, H7), 7.33 (dd, 1H, J = 7.3, 1.4 Hz, H4), 7.32 (td, 1H, J = 7.2, 1.6 Hz, H6), 7.15 (td, 1H, J = 7.5, 1.2 Hz, H5), 6.58 (s, 1H, H8a), 4.03 (s, 3H, OMe), 3.90 (s, 3H, COOMe), 2.10 and 1.99 (2dq, 2H, J = 14.3, 7.4 Hz, CH_2), 0.92 (t, 3H, J = 7.4 Hz, Me). ^{13}C NMR (75 MHz, acetone-d_6): δ 170.9 (s, C2), 154.2 (s, NCO), 141.8 (s, C7a), 136.1 (s, C3b), 130.2 (d, C6), 125.6 (d, C5), 124.0 (d, C4), 116.9 (s, CN), 116.5 (d, C7), 98.9 (d, C8a), 63.6 (s, C3), 59.8 (s, C3a) 59.5 (q, OMe), 54.4 (q, COO*Me*), 29.7 (t, CH_2), 9.3 (q, Me).

4b. ^{1}H NMR (300 MHz, acetone-d_6): δ 7.92 (br s, 1H, H7), 7.50 (dd, 1H, J = 7.6, 1.4 Hz, H4), 7.44 (td, 1H, J = 7.5, 1.5 Hz, H6), 7.14 (td, 1H, J = 7.5, 1.0 Hz, H5), 5.55 (s, 1H, H8a), 4.00 (s, 3H, OMe), 3.82 (s, 3H, COOMe), 2.32 and 2.19 (2dq, 2H, J = 14.2, 7.3 Hz, CH_2), 0.97 (t, 3H, Me). ^{13}C NMR (75 MHz, acetone-d_6): δ 173.5 (s, C2), 153.8 (s, NCO), 143.8 (s, C7a), 132.9 (d, C6), 130.4 (s, C3b), 126.0 (d, C4), 124.9 (d, C5), 116.8 (d, C7), 116.4 (s, CN), 98.2 (s, C3a), 69.7 (d, C8a), 60.2 (s, C3), 59.1 (q, OMe), 53.5 (q, COO*Me*), 31.1 (t, CH_2), 8.3 (q, Me).

5b. Pure sample was obtained by recrystallization from a mixture of CH_2Cl_2/hexane to give colorless crystals. Mp: 137−138 °C. R_f: 0.42 (CH_2Cl_2). IR ($CHCl_3$): ν_{max} 3028, 2252, 1752, 1606 cm^{-1}. ^{1}H NMR (300 MHz, acetone-d_6): δ 8.21 (dt, 1H, J = 8.3, 0.8, H7), 7.74 (dd, 1H, J = 7.8, 1.4 Hz, H4), 7.46 (td, 1H, J = 7.2, 1.4 Hz, H6), 7.37 (td, 1H, J = 7.7, 1.1 Hz, H5), 6.00 (s, 1H, H8), 4.10 (s, 3H, NCOOMe), 3.84 (s, 3H, COOMe), 2.92 (qi, 2H, J = 2.2 Hz, CH_2), 1.28 (t, 3H, J = 7.4 Hz, Me). ^{13}C NMR (75 MHz, acetone-d_6): δ 166.5 (s, C*CO*), 153.1 (s, NCO), 137.5 (s, C7a), 130.2 (s, C3a), 128.3 (s, C3), 127.4 (d, C6), 125.3 (s, C2), 125.0 (d, C5), 121.0 (d, C4), 117.3 (d, C7), 116.6 (s, CN), 55.1 (q, NCOO*Me*), 54.6 (q, COO*Me*), 37.6 (d, C8), 18.3 (t, CH_2), 15.9 (q, Me). MS (EI), m/z: (relative inensity) 300 (M^+, 48), 268 (100), 241 (186). HRMS (FAB), m/z: 323.1011 (M^+, $C_{16}H_{16}N_2O_4$ + Na requires 323.1008).

Methyl 3a-Benzyl-3-cyano-2-methoxy-3a*H*-furo[2,3-*b*]indole-8(8a*H*)-carboxylate (2c), Methyl 8b-Benzyl-3-cyano-2-methoxy-3a*H*-furo[3,2-*b*]indole-4(8b*H*)-carboxylate (4c), and Methyl 3-Benzyl-2-(1-cyano-2-methoxy-2-oxoethyl)-1*H*-indole-1-carboxylate (5c). Following the general procedure, reaction of furoindoline **1c** with diazomethane gave a colorless oil mixture of isomeric products **2c** and **4c** in proportions of 9:1 in an overall >99% yield. This material was standing at 22 °C in DMSO (1 mL) until its complete transformation (8 h) and then concentrated to dryness to afford pure enough indole **5c** as colorless crystals in >99% yield.

2c. Pure sample was obtained by recrystallization from a mixture of ether/hexane to give colorless crystals. Mp: 115−116 °C. ^{1}H NMR (300 MHz, acetone-d_6): δ 7.74 (br s, 1H, H7), 7.53 (m, 1H, H4), 7.35 (td, 1H, J = 7.7, 1.4 Hz, H6), 7.31−7.27 (m, 5H, Ar), 7.21 (td, 1H, J = 7.4, 1.1 Hz, H5), 6.63 (s, 1H, H8a), 3.91 (s, 3H, OMe), 3.82 (s, 3H, COOMe), 3.48 and 3.25 (2d, 2H, J_{AB} = 13.8 Hz, CH_2). ^{13}C NMR (75 MHz, acetone-d_6): δ 171.1 (s, C2), 153.8 (s, NCO), 141.8 (s, C7a), 136.9 (s, C_i), 136.1 (s, C3b), 131.7 (d, C_o), 130.0 (d, C6), 129.9 (d, C_p), 128.6 (d, C_m), 125.6 (d, C5), 124.2 (d, C4), 116.6 (s, CN), 116.6 (d, C7), 98.4 (d, C8a), 64.2 (s, C3), 60.2 (s, C3a), 59.4 (q, OMe), 54.4 (q, COO*Me*), 42.1 (t, CH_2).

4c. Due to the reaction progress, the spectral NMR data of **4c** listed below stem from the 1:1 mixture of **2c** and **4c** for ^{1}H and from the 1:2 mixture for ^{13}C. ^{1}H NMR (300 MHz, acetone-d_6): δ 7.91 (br s, 1H, H7), 7.54 (dd, 1H, J = 7.7, 1.4 Hz, H4), 7.45 (m, 1H, H6), 7.39−7.33 (m, 5H, Ar), 7.16 (td, 1H, J = 7.4, 0.8 Hz, H5), 5.58 (s, 1H, H8a), 3.97 (s, 3H, OMe), 3.77 (s, 3H, COOMe), 3.70 and 3.44 (2d, 2H, J_{AB} = 13.8 Hz, CH_2). ^{13}C NMR (75 MHz, acetone-d_6): δ 173.1 (s, C2), 153.7 (s, NCO), 143.8 (s, C7a), 135.4 (s, C_i), 132.9 (d, C6), 132.0 (d, C_o), 130.5 (d, C_p), 130.3 (s, C3b), 129.0 (d, C_m), 126.4 (d, C4), 124.7 (d, C5), 116.7 (s, CN), 116.5 (d, C7), 96.9 (s, C3a), 69.8 (d, C8a), 60.4 (s, C3), 59.1 (q, OMe), 53.5 (q, COO*Me*), 43.5 (t, CH_2).

5c. Pure sample was obtained by recrystallization from a mixture of CH_2Cl_2/hexane to give colorless crystals. Mp: 144−145 °C. R_f: 0.39 (CH_2Cl_2). IR ($CHCl_3$): ν_{max} 3024, 2254, 1756, 1604 cm^{-1}. ^{1}H NMR (300 MHz, acetone-d_6): δ 8.22 (dt, 1H, J = 8.4, 0.9, H7), 7.56 (dd, 1H, J = 7.8, 1.3 Hz, H4), 7.43 (td, 1H, J = 7.2, 1.3 Hz, H6), 7.36−7.22 (m, 5H, Ar), 7.28 (td, 1H, J = 7.2, 0.9 Hz, H5), 6.11 (s, 1H, H8), 4.36 and 4.29 (2d, 2H, J_{AB} = 16.2, CH_2), 4.13 (s, 3H, NCO_2Me), 3.85 (s, 3H, COOMe). ^{13}C NMR (75 MHz, acetone-d_6): 166.4 (s, C*CO*), 153.1 (s, NCO), 140.7 (s, C_i), 137.6 (s, C7a), 130.1 (s, C3a), 130.0 (d, C_m), 129.9 (d, C_o), 127.9 (d, C_p), 127.5 (d, C6), 126.8 (s, C2), 125.1 (s, C3), 125.0 (d, C5), 121.7 (d, C4), 117.3 (d, C7), 116.4 (s, CN), 55.2 (q, NCOO*Me*), 54.7 (q, COO*Me*), 37.9 (d, C8), 30.6 (t, CH_2). MS (EI), m/z: (relative inensity) 362 (M^+, 55), 330 (47), 264 (100), 243 (49). HRMS (FAB), m/z: 385.1172 (M^+, $C_{21}H_{18}N_2O_4$ + Na requires 385.1172).

Methyl 3-Cyano-3a-isopropyl-2-methoxy-3a*H*-furo[2,3-*b*]indole-8(8a*H*)-carboxylate (2d), Methyl 3-Cyano-8b-isopropyl-2-methoxy-3a*H*-furo[3,2-*b*]indole-4(8b*H*)-carboxylate (4d), and Methyl 2-(1-Cyano-2-methoxy-2-oxoethyl)-3-isopropyl-1*H*-indole-1-carboxylate (5d). Following the general procedure, reaction of

furoindoline **1d** with diazomethane gave compound **2d** as colorless oil in >99% yield.

2d. Pure sample was obtained by silica gel chromatography with CH_2Cl_2/hexane (1:1) to give a colorless oil. R_f: 0.40 (CH_2Cl_2). IR (CH_2Cl_2): ν_{max} 3058, 2202, 1728, 1656, 1602 cm^{-1}. ^1H NMR (300 MHz, acetone-d_6): δ 7.83 (br s, 1H, H7), 7.37 (dd, 1H, J = 7.2, 1.4 Hz, H4), 7.36 (td, 1H, J = 7.4, 1.4 Hz, H6), 7.19 (td, 1H, J = 7.4, 1.1 Hz, H5), 6.60 (s, 1H, H8a), 4.05 (s, 3H, OMe), 3.93 (s, 3H, COOMe), 2.47 (h, 1H, J = 6.9 Hz, *i*-Pr), 1.18 (d, 3H, J = 6.9 Hz, *i*-Pr), 0.76 (d, 3H, J = 6.9 Hz, *i*-Pr). ^{13}C NMR (75 MHz, acetone-d_6): δ 170.8 (s, C2), 154.1 (s, NCO), 141.9 (s, C7a), 135.9 (s, C3b), 130.3 (d, C6), 125.7 (d, C5), 123.9 (d, C4), 116.6 (d, C7), 116.5 (s, CN), 96.4 (d, C8a), 68.8 (s, C3), 63.9 (s, C3a), 59.5 (q, OMe), 54.5 (q, COO*Me*), 33.3 (d, CH), 18.4 (q, Me), 17.5 (q, Me).

Isolation of 4d. Compound **2d** (0.08 mmol) was allowed to stand at room temperature in DMSO (0.5 mL) until ca. 50% conversion of **2d** was achieved (3 h). The reaction mixture was diluted with CH_2Cl_2 (10 mL), and the organic phase was washed with brine (12 × 1 mL). Removal of the solvent under an argon stream led to an oil residue which was chromatographed over a short path of silica gel (10 cm, column 50 × 1.5 cm) eluted with hexane/CH_2Cl_2 3:2. The fractions containing **4d** were collected (25 mL) and concentrated in vacuo at 40 °C to afford the pure compound as a colorless oil in 27% yield. Pure sample was obtained by recrystallization from a mixture of CH_2Cl_2/hexane to give colorless crystals. Mp: 122−124 °C. R_f: 0.16 (CH_2Cl_2). IR (CH_2Cl_2): ν_{max} 3080, 2210, 1716, 1640, 1604 cm^{-1}. ^1H NMR (300 MHz, acetone-d_6): δ 7.93 (br s, 1H, H7), 7.49 (dd, 1H, J = 7.7, 1.5 Hz, H4), 7.45 (td, 1H, J = 7.4, 1.5 Hz, H6), 7.15 (td, 1H, J = 7.5, 1.0 Hz, H5), 5.60 (s, 1H, H8a), 4.02 (s, 3H, OMe), 3.83 (s, 3H, COOMe), 2.67 (h, 1H, J = 6.8 Hz, *i*-Pr), 1.09 (d, 3H, J = 6.5 Hz, *i*-Pr), 0.82 (d, 3H, J = 7.1 Hz, *i*-Pr). ^{13}C NMR (75 MHz, acetone-d_6): δ 173.3 (s, C2), 153.7 (s, NCO), 143.7 (s, C7a), 132.9 (d, C6), 130.3 (s, C3b), 126.0 (d, C4), 125.0 (d, C5), 116.8 (d, C7), 116.7 (s, CN), 100.8 (s, C3a), 67.2 (d, C8a), 60.6 (s, C3), 59.2 (q, OMe), 53.5 (q, COO*Me*), 35.4 (d, CH), 17.2 (q, Me), 16.5 (q, Me).

5d. Compound **4d** was standing at 22 °C in DMSO (1 mL) until its complete transformation (20 h) and then concentrated to dryness to afford the pure enough indole **5d** as colorless oil in >99% yield. Pure sample was obtained by recrystallization from a mixture of CH_2Cl_2/hexane to give colorless crystals. Mp: 163−165 °C. R_f: 0.38 (CH_2Cl_2). IR ($CHCl_3$): ν_{max} 3020, 2252, 1754, 1602 cm^{-1}. ^1H NMR (300 MHz, acetone-d_6): δ 8.24 (dt, 1H, J = 8.5, 1.1, H7), 7.92 (dd, 1H, J = 8.0, 1.4 Hz, H4), 7.44 (td, 1H, J = 7.1, 1.4 Hz, H6), 7.34 (td, 1H, J = 7.7, 1.1 Hz, H5), 6.08 (s, 1H, H8), 4.10 (s, 3H, NCOOMe), 3.85 (s, 3H, COOMe), 3.45 (h, 1H, J = 7.1 Hz, *i*-Pr), 1.50 (d, 3H, J = 6.9 Hz, *i*-Pr), 1.49 (d, 3H, J = 7.1 Hz, *i*-Pr). ^{13}C NMR (75 MHz, acetone-d_6): δ 166.5 (s, C*CO*), 153.1 (s, NCO), 138.0 (s, C7a), 131.5 (s, C3), 129.0 (s, C3a), 127.1 (d, C6), 124.7 (d, C4), 124.6 (s, C2), 122.7 (d, C4), 117.4 (d, C7), 116.7 (s, CN), 55.1 (q, NCOO*Me*), 54.7 (q, COO*Me*), 37.5 (d, C8), 27.5 (d, CH), 23.1 (q, Me), 22.9 (q, Me). MS (EI), *m*/*z*: (relative inensity) 314 (M^+, 72), 282 (67), 267 (100), 255 (62). HRMS (FAB) *m*/*z*: 337.1175 (M^+, $C_{17}H_{18}N_2O_4$ + Na requires 337.1164).

Methyl 3-Cyano-3a-*tert*-butyl-2-methoxy-3a*H*-furo[2,3-*b*]indole-8(8a*H*)-carboxylate (2e), Methyl 3-Cyano-8b-*tert*-butyl-2-methoxy-3a*H*-furo[3,2-*b*]indole-4(8b*H*)-carboxylate (4e), and Methyl 2-(1-Cyano-2-methoxy-2-oxoethyl)-3-*tert*-butyl-1*H*-indole-1-carboxylate (5e). Following the general procedure, reaction of furoindoline **1e** with diazomethane gave compound **2e** as colorless oil in >99% yield.

2e. Pure sample was obtained by recrystallization from a mixture of CH_2Cl_2/hexane to give colorless crystals. Mp: 130−132 °C. R_f 0.43 (CH_2Cl_2). IR (CH_2Cl_2): ν_{max} 3058, 2202, 1728, 1646, 1602 cm^{-1}. ^1H NMR (300 MHz, acetone-d_6): δ 7.85 (br s, 1H, H7), 7.54 (dd, 1H, J = 7.4, 1.1 Hz, H4), 7.38 (td, 1H, J = 7.4, 1.4 Hz, H6), 7.20 (td, 1H, J = 7.7, 1.1 Hz, H5), 6.62 (s, 1H, H8a), 4.01 (s, 3H, OMe), 3.95 (s, 3H, COOMe), 1.13 (s, 9H, 3Me). ^{13}C NMR (75 MHz, acetone-d_6): δ 172.5 (s, C2), 153.9 (s, NCO), 142.2 (s, C7a), 134.8 (s, C3b), 130.2 (d, C6), 126.5 (d, C4), 125.3 (d, C5), 117.9 (s, CN), 116.9 (s, C7), 98.5 (d, C8a), 65.5 (s, C3a), 62.4 (s, C3), 59.3 (q, OMe), 54.6 (q, COO*Me*), 37.8 (s, C), 26.5 (q, 3Me).

Isolation of 4e. Compound **2e** (0.08 mmol) was standing at room temperature in DMSO (0.5 mL) until ca. 80% conversion of **2e** was achieved (48 h). The reaction mixture was diluted with CH_2Cl_2 (10 mL), and the organic phase was washed with brine (12 × 1 mL). Removal of the solvent under an argon stream led to an oily residue which was chromatographed over a short path of silica gel (10 cm, column 50 × 1.5 cm) eluted with hexane/CH_2Cl_2 3:2. The fractions containing **4e** were collected (25 mL) and concentrated in vacuo at 40 °C to afford the pure compound as a colorless oil in 58% yield. Pure sample was obtained by recrystallization from a mixture of CH_2Cl_2/hexane to give colorless crystals. Mp: 160−162 °C. R_f: 0.20 (CH_2Cl_2). IR (CH_2Cl_2): ν_{max} 3070, 2208, 1716, 1644, 1602 cm^{-1}. ^1H NMR (300 MHz, acetone-d_6): δ 7.95 (br s, 1H, H7), 7.55 (dd, 1H, J = 7.8, 1.3 Hz, H4), 7.44 (td, 1H, J = 7.5, 1.3 Hz, H6), 7.13 (td, 1H, J = 7.5, 1.1 Hz, H5), 5.71 (s, 1H, H8a), 4.04 (s, 3H, OMe), 3.83 (s, 3H, COOMe), 1.09 (s, 9H, 3 Me). ^{13}C NMR (75 MHz, acetone-d_6): δ 173.0 (s, C2), 153.6 (s, NCO), 143.6 (s, C7a), 132.6 (d, C6), 129.7 (s, C3b), 127.9 (d, C4), 124.6 (d, C5), 116.9 (d, C7), 116.4 (s, CN), 101.8 (s, C3a), 68.7 (d, C8a), 60.3 (s, C3), 59.1 (q, OMe), 53.6 (q, COO*Me*), 38.9 (s, C), 24.8 (q, 3Me).

5e. Compound **4e** was standing at 22 °C in DMSO (1 mL) until its complete transformation (480 h) and then concentrated to dryness to afford indole **5e** as a colorless oil in >99% yield. Pure sample was obtained by recrystallization from a mixture of CH_2Cl_2/hexane to give white solid. Mp: 118−120 °C. R_f: 0.39 (CH_2Cl_2). IR ($CHCl_3$) ν_{max} 3030, 2252, 1752, 1586 cm^{-1}. ^1H NMR (300 MHz, acetone-d_6): δ 8.25 (ddd, 1H, J = 8.5, 1.2, 0.8 Hz, H7), 8.07 (dd, 1H, J = 8.2, 1.1, 0.6 Hz, H4), 7.42 (td, 1H, J = 7.1, 1.1 Hz, H6), 7.33 (td, 1H, J = 7.4, 1.4 Hz, H5), 6.28 (s, 1H, H8), 4.09 (s, 3H, NCO_2Me), 3.89 (s, 3H, COOMe), 1.68 (s, 9H, 3Me). ^{13}C NMR (75 MHz, acetone-d_6): δ 166.5 (s, C*CO*), 153.2 (s, NCO), 137.9 (s, C7a), 133.0 (s, C3), 129.8 (s, C3a), 126.8 (d, C6), 124.6 (d, C4), 124.3 (d, C5), 124.3 (s, C2), 117.1 (s, C7), 117.0 (d, CN), 55.2 (q, NCOO*Me*), 54.6 (q, CCOO*Me*), 38.9 (d, C8), 35.5 (s, C), 32.7 (q, 3Me). MS (EI), *m*/*z*: (relative intensity) 328 (M^+, 20), 282 (81), 241 (100). HRMS (FAB), *m*/*z*: 329.1497 (M^+, $C_{17}H_{18}N_2O_4$ + H requires 329.1501).

NMR Kinetic Experiments. ^1H NMR studies (300 MHz) were carried out in duplicated with a substrate concentrations of 0.03−0.04 mmol/mL of DMSO-d_6 solvent. The time interval between two successive experiments was dependent on the rate of rearrangement in order to collect a number of data points for accurate rate determination (12−25 registered spectra). All reactions were monitored up to 80% conversion of starting material (from 0.50 to 76 h). Analyses of **2a** and **2c** were carried out at 295 K; for **2b** at 295, 303, and 310 K; for **2d** at 295, 303, 310, and 319 K; for **2e** at 295, 303, 311, 319 K; for **4d** at 295, 301, 311, and 319 K; and for **4e** at 308, 318, and 328 K. After the experiments in a kinetic run were finished, they were all integrated serially. The singlet or singlets corresponding to the methine proton or protons in the first experiment of the series were normalized to 100% and the integrals of the singlet methine peaks appearing in successive experiments were measured against the first experiment. The residual solvent peaks from DMSO-d_6 (at 2.56 ppm) served as an internal standard for this analysis: the combined integrals for products and starting material methine singlets were constant relative to the DMSO-d_6 methyl groups over the course of the reaction.

Acknowledgment. Financial support by CONACYT Grant No. 8180 is gratefully acknowledged. This work is part of the doctoral thesis of P.Y.L.C.

Supporting Information Available: Copies of ^{1}H and ^{13}C NMR spectra for all new compounds and tables of all observed gHSQC and gHMBC interactions used for assignment. X-ray crystallographic data for compounds **2e**, **3c**, **4d**, and **4e**. Kinetic data (rate constants of individual kinetic runs). Cartesian coordinates, total energies, thermochemistry, and variational PCM results (DMSO) for calculated molecules and transition structures. This material is available free of charge via the Internet at http://pubs.acs.org.